# Provenance and composition of unusually chrome and nickel-rich bucket-shaped pottery from Rogaland (southwestern Norway)

Udo Zimmermann [a,*], Elna Siv Kristoffersen [b], Per Ditlef Fredriksen [c,d], Silvana A.R. Bertolino [e], Sergio Andò [f], Danilo Bersani [g]

[a] University of Stavanger, Department of Petroleum Engineering, Ullandhaug, 4036 Stavanger, Norway
[b] University of Stavanger, Museum of Archaeology, 4036 Stavanger, Norway
[c] University of Oslo, Department of Archaeology, Conservation and History, 0315 Oslo, Norway
[d] University of Cape Town, Department of Archaeology, Rondebosch 7701, South Africa
[e] Universidad Nacional de Córdoba, FaMAF, Medina Allende s/n, Ciudad Universitaria, Córdoba, Argentina
[f] University of Milano-Bicocca, Department of Earth and Environmental Science, Piazza della Scienza 4, 20126 Milano, Italy
[g] University of Parma, Dipartimento di Fisica e Scienze della Terra, Parco Area delle Scienze, 7/A, 43124 Parma, Italy

## ARTICLE INFO

## ABSTRACT

We report results from FE-SEM–EDS, geochemical, mineralogical analyses and Raman spectroscopy of pottery of bucket-shaped ceramic from Rogaland (southwestern Norway) dated between the 5th and 6th Century. The study reveals a very rare pottery composition including asbestos-group minerals and an unusual enrichment in compatible elements like Cr ($8–27\times$ Post Archean average shale (PAS), McLennan et al., 2006), Ni ($2–8\times$ normal shale) and Co ($2–3\times$ PAS). X-Rray diffraction and Raman spectroscopy could pinpoint that Ni is introduced by specific Ni-rich talc mineral and chlorite minerals and Cr occurs in a rare Cr-rich talc, and possibly in a Cr-chlorite, these minerals are the most abundant in the pottery, which is supported by strong enrichment in Mg ($10–20\times$ PAS). The addition of Mg, Cr, Ni and Co and other compatible trace elements is to our current knowledge not caused by anthropogenic activity but related to the used materials, which are alteration products of mafic and ultramafic rocks or genetically related to mafic and ultramafic rocks. Rocks of this type are exposed in vicinity of the sampling areas in a region called Karmøy, hosting a world famous ophiolite complex, which is identified as the major source for the mafic and ultramafic component, as the next succession of a similar composition is far further north located in Norway and a number of rock types on Karmøy matches the chemical composition of the pottery. The here reported composition is spectacular and extremely rare – if ever found – in pottery. Our study shows that unusual material sources have been used in pottery production, and this opens for discussion whether the materials were deliberately selected by the manufacturers, thereby expressing a specific social function, in a time period where more functional clay types and additives, and certainly functional and sufficient for use in pottery, where abundant in areas of Rogaland closer to where the pots were found.

© 2015 Elsevier B.V. All rights reserved.

## 1. Introduction

During the 6th century AD in southwest Norway (Fig. 1), a short peak/collapse phase characterized the development of sophisticated ceramic handcraft (Fig. 2), which went from flourishing to nothing in a few decades. In the two centuries spanning c. AD 350–550, which included the last decades of the Late Roman Iron Age (LRIA, AD 200–400) and the entire Migration Period (MP, AD 400–550), the manufacturing of the ceramic type known as bucket-shaped was highly characteristic. Moreover, it seems this ceramic production ceased concurrently with that of distinguished gold/gilded objects decorated with the Animal Art style known as Style I (Fredriksen et al., 2014). The bucket-shaped pots occur in almost every grave during this period, as well as in residential contexts. The typological development of these pots is of central importance to the chronological phasing of the period in western Scandinavia (Kristoffersen and Magnus, 2010, with references). Early bucket shaped pots are decorated with simple ornaments as lines and finger formed knobs, while during a transition period more sophisticated ornaments were developed, as the interlaced pattern. The final stage represents sophisticated pots with fine ornamentation (Kristoffersen and Magnus, 2010). Rogaland (Fig. 1) seems to be a core area with by far the largest find concentration. Several art and or craft traditions seem to have been established in the Migration Period, which stands out as an active and experimental artistic period, a development that had been contributed to and affected by social and political changes in the society (Fredriksen et al., 2014).

* Corresponding author. Tel.: +47 51832270, fax: +47 51831750.
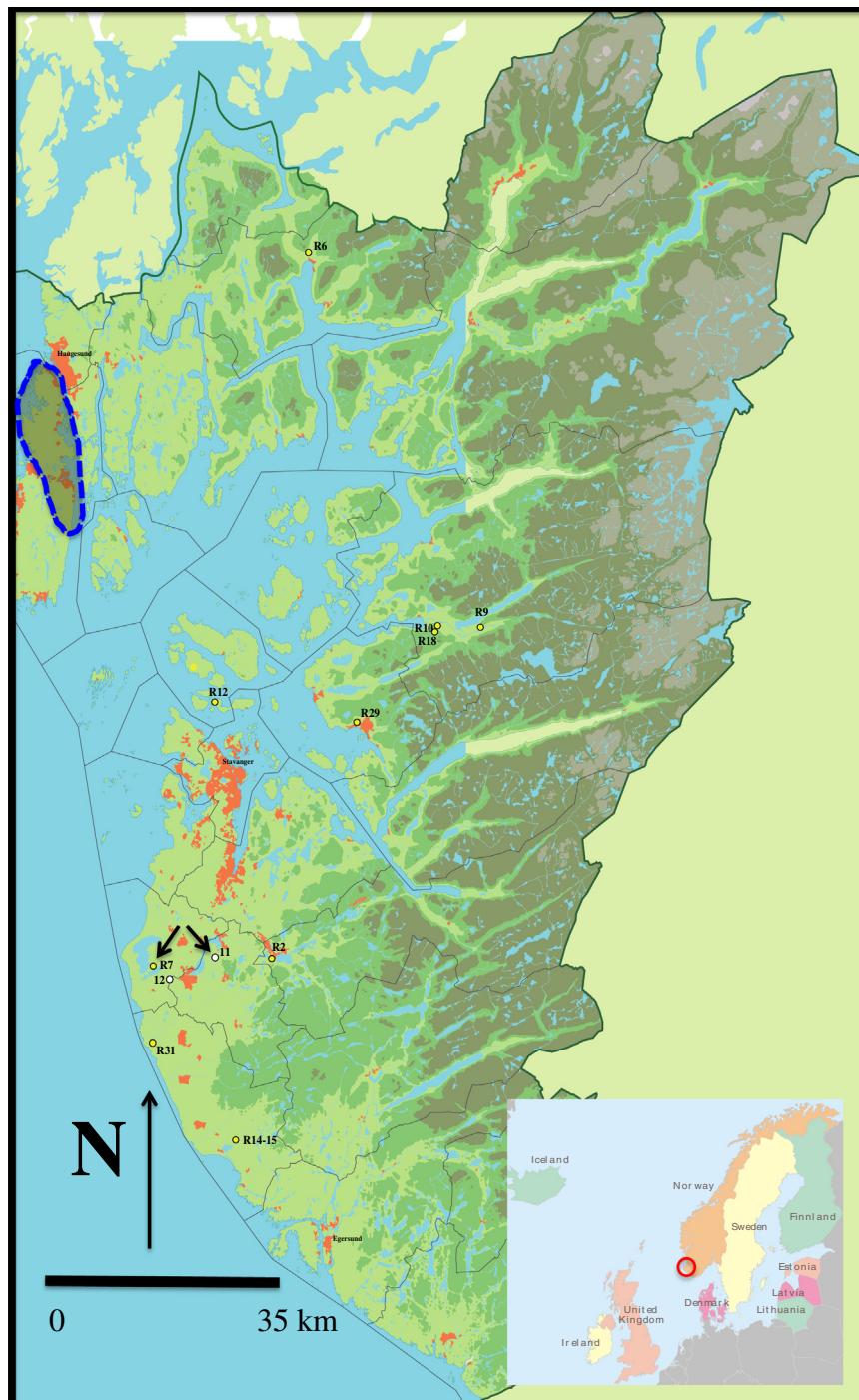E-mail address: udo.zimmermann@uis.no (U. Zimmermann).

**Fig. 1.** Geographic sketch map with the sample locations in southwest Norway around the town Stavanger. The red circle in the small inlet indicates the study area. Encircled with stippled blue line the proposed source area for the used mafic to ultramafic component from Karmøy for the manufacturing of the pottery. The two black arrows show the unique samples in this study with a non-ultramafic composition.

This study wanted to test the potential of archaeometric techniques for this type of ceramics. We show, within this contribution, that the application of optical petrography, geochemistry (ICP-MS studies on pottery sherds), X-ray diffraction, Field emission scanning electron microscopy with semi-quantitative chemistry (FE-SEM–EDS) combined with non-destructive Raman spectroscopy yields in revealing the composition and the origin of the used materials. The extraordinary results in this study allow in speculating about the social strategies of using the specific materials.

### 1.1. The objects of study

Although bucket-shaped is a *Leitfossil* for the Migration Period, and especially the period's two last phases, (AD 450–500 and AD 500–550) this study focuses on the first century of bucket-shaped pottery production. For this pilot study we selected thirteen pottery samples from the LRIA (AD 350–400) and the first phase of the MP (AD 400–450) from Rogaland (Fig. 1), following Kristoffersen and Magnus' (2010) most recent ceramic sequence. The samples are from graves
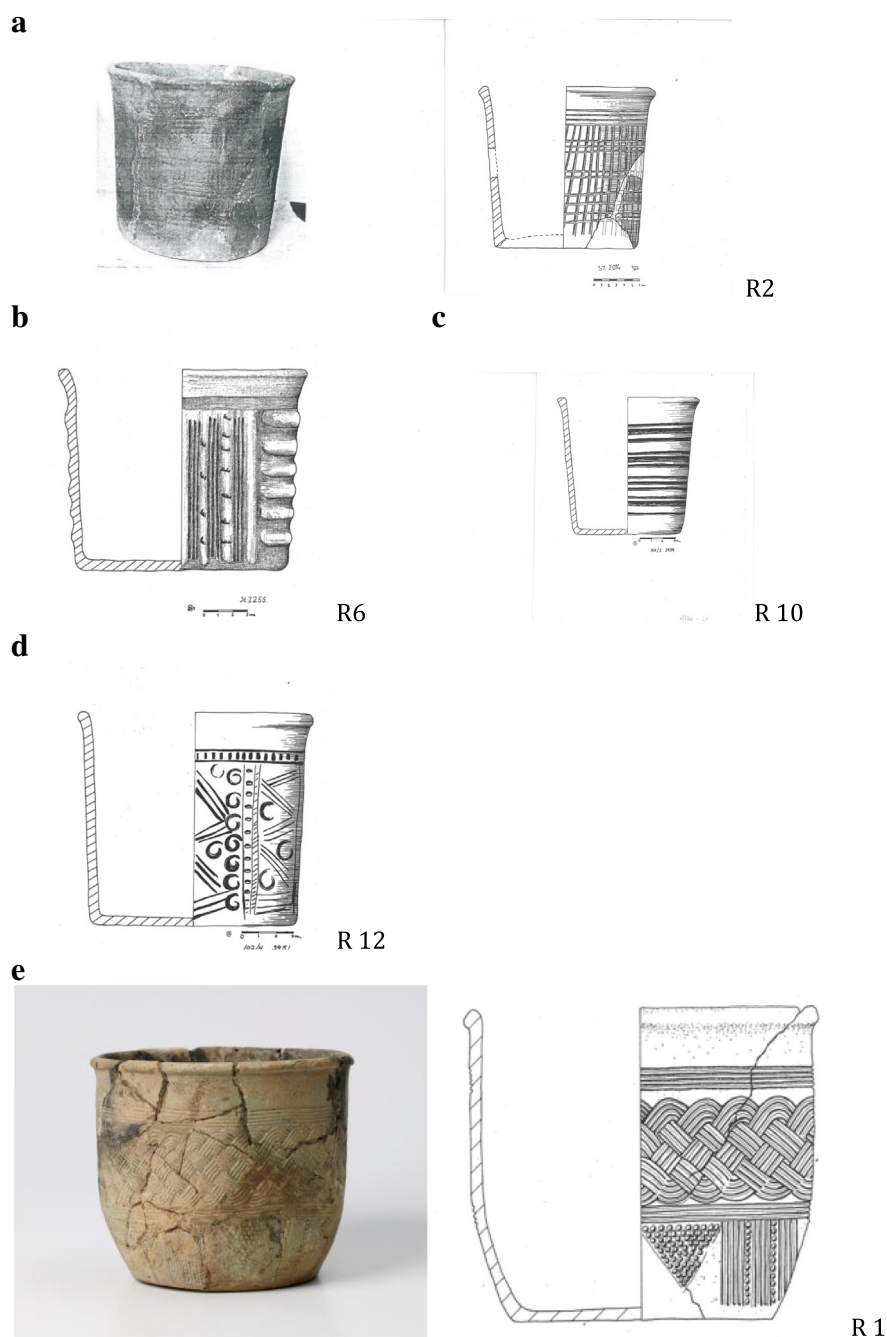
**Fig. 2.** Examples of bucket-shaped pots used in this study. a) R2 Edland, Gjesdal (S2014); b) R6 Østabø, Vindafjord (S2255); c) R10 Soppaland, Hjelmeland (S2759); d) R12 Heigreberg, Rennesøy (S2951) information see chapter 'Sampling and methodology'; e) Example for high quality pots from Lima, Gjesdal (sample R1, S1440), Late phase.

(Fig. 2) and settlement sites. The type is made of fired clay and is thus clearly pottery, although the small proportion of clay in relation to additives is unusual. Also, the shaping technique is unique, at least for contemporary South and Central Scandinavia. In contrast to most contemporary pottery, which is made by coiling in the so-called N technique, bucket-shaped vessels were made by a distinct plate-and-mold technique. As firmly established by experiments (Kleppe and Simonsen, 1983), the potter first prepared a thin rectangular plate and a circular bottom piece. Then the plate was shaped upside-down around a mold of wood or clay, and joint with the bottom plate. The vessel was decorated while still on the mold. Detailed information about the samples can be found in chapter 'Sampling and Methodology' and Table 1.

The bucket-shaped pots seem to have had a central ritual significance in mortuary practice and may have been made special for this purpose. That does not, however, exclude their importance in household and daily life (Fredriksen et al., 2014). Several vessels found in burials show evidence of repair, a fact that reflects their significance as objects with life histories before being deposited with the deceased (Magnus, 1980). From the household contexts there is also another type of more practical pots, which do not occur in graves, larger pots with coarser ware. In addition, in both household and grave contexts there are finer black burnished pots of yet another type that differs in production mode, fabric, form and ornamentation. All these different types of pots were in use concurrently with the early phase of bucket-shaped pots. Also, it should be pointed out here that the ceramic type most probably originated as part of changes in food practice during the LRIA (Kleppe, 1993; Kleppe and Simonsen, 1983), but its functionality seems to have altered some time after the early phase discussed

**Table 1**
Compilation of general data for the pottery fragments used in this study. 'gnr.' indicates the 'cadastral number'; 'K' indicates 'municipality'; GC = geochemistry; XRD = X-ray diffraction. AB1, AB2, AB4 and C relates to types of bucket shaped pots (see Kristoffersen and Magnus, 2010).

| Locality | Sample | Locality and register | Typology | Function of sample | GC | Raman | XRD | FE-SEM |
|---|---|---|---|---|---|---|---|---|
| Gjesdal | R2 | S2014 Edland gnr. 5 | Cylindrical/irregular, incised (AB4) | Ritual/grave | x | | x | x |
| Vindafjord | R6 | S2255 Østebø gnr. 9 | Cylindrical/relief (cordons) (AB1) | Ritual/grave | x | | x | x |
| Klepp | R7 | S2311c Erga gnr. 30 | Body shard/finger-tip shaped bosses | Ritual/grave | x | | x | x |
| Hjelmeland | R9 | S2549a Rivjaland gnr. 127 | Body shard/comb bands | Ritual/grave | x | x | x | x |
| Hjelmeland | R10 | S2759 Soppaland gnr. 138 | Concave/horizontal, incised bands (AB2) | Ritual/grave | x | x | x | x |
| Rennesøy | R12 | S2951 Heigreberg gnr. 43 | Cylindrical/incised cevrons, circular stamp marks (AB1) | Ritual/grave | x | x | x | x |
| Hå | R14 | S4059a Fuglestad gnr. 111 | Cylindrical/irregular, incised (AB4 or AB1) | Ritual/grave | x | x | x | x |
| Hå | R15 | S4059a Fuglestad gnr. 111 | R14 and R15 are from the same pot | Ritual/grave | x | | x | x |
| Hjelmeland | R18 | S4476e Soppaland gnr. 138 | Convex (transitional phase?)/comb bands, stamp marks (C?) | Ritual/grave | x | | x | x |
| Strand | R29 | S6580e Barka gnr. 42 | Rim shard/finger-tip shaped bosses | Ritual/grave | x | | x | x |
| Hå | R31 | S6754f Obrestad gnr. 11 | Body shard | Household | x | | x | x |
| Time | 11 | 4190e Netland gnr. 26 | Large shard: cylindrical/incised, cevrons, comb staming (A1?) | Ritual/grave | x | | x | x |
| Time | 12 | 6121b Hanaland gnr. 3 | Cylindrical/comb bands, cevrons, circular stamp marks (A1) | Ritual/grave | x | x | x | x |

here. This is most probably linked to the introduction of the iron band below the rim, which was attached to a handle. The iron band became a regular feature during the second phase of the MP (AD 450–500). The pot thereby changed functionality from hand-held/standing to hanging/standing.

Hence, in this study nearly each sample has a specific context and similarities are observed to be intentionally. Differences of the samples would be expected because of the handmade production process, which would reflect slight differences in composition, including the use of different amounts of components, natural variation of the used materials and differing post-burial histories controlled by natural processes or anthropogenic influences.

## 2. Sampling and methodology

### 2.1. Sampling

We selected 13 samples as being representative for the early phase of the bucket-shaped ceramic in Rogaland for this pilot study (see Table 1; Figs. 1, 2). The sample selection has been based on meticulous studies by Kristoffersen and Magnus (2010) and covers therefore the necessary variety in style, locality and grave type. The samples are taken from the deposit of the Museum of Archaeology, University of Stavanger and Table 1 refers to the detailed cataloged description of the samples. The samples were cleaned, with a dry cloth without leaving any fabric particles and soft blow of pressed air, from any dust and soil to avoid contamination caused during their depositional time in the sampling site or during conservation.

### 2.2. Optical petrography

Covered thin sections of early phase pottery have been studied by using a Leica, type 020–520.007DM/LP at the University of Milano-Bicocca with magnification of 4×, 10×, 20× and 63×.

### 2.3. Field emission scanning electron microscopy with energy dispersive system (FE-SEM–EDS)

Surfaces of freshly broken chips of the samples (Table 1) coated with palladium were imaged using a Zeiss Supra 35VP field emission SEM in high vacuum mode with an accelerating voltage of 10 kV. EDAX Genesis energy-dispersive X-ray spectroscopy (EDS) was applied for determining the semi-quantitative elemental and mineralogical composition of the samples (Bertolino et al., 2009).

### 2.4. X-ray diffraction

Samples of c. 0.5 to 1 g have been crushed by hand in an agate mortar to fine mesh of micron size, and were loaded in random mounts to be analyzed on a Philips X'Pert PRO PW 3040/60 diffractometer, with Cu Kα X-ray radiation, Si monochromator, at 40 kV and 30 mA. Step scan at ~1°/min and step size of 0.02° 2θ. A silicon background zero sample holder was used for smaller samples (few milligrams) as for R7. HighScore Plus version 3.0d PANanalytical software (DEgen et al., 2014) with ICDD PDF2 database was used for mineral identification.

### 2.5. Geochemistry

Samples were processed and pulverized to very fine mesh (<2 μm) in an ultraclean agate mill. Geochemical data were obtained using ICP-MS analysis at Acme laboratory (Vancouver, Canada). Detection limits are given in Table 3. Details for the analytical method and processing can be found in http://acmelab.com and are compiled here: The samples have been milled in an agate mill. The prepared sample is mixed with $LiBO_2/Li_2B_4O_7$ flux. Crucibles are fused in a furnace. The cooled bead is dissolved in ACS grade nitric acid and analyzed by ICP-MS. Loss on ignition (LOI) is determined by igniting a sample split then measuring the weight loss. A 1 g sample is weighed into a tarred crucible and is ignited to 1000 °C for one hour, cooled and weighed. The loss in weight is the LOI of the sample. Total Carbon and Sulfur may be included and are determined by the Leco method. Here, induction flux is added to the prepared sample then ignited in an induction furnace. A carrier gas sweeps up released carbon to be measured by adsorption in an infrared spectrometric cell. Results are total and attributed to the presence of carbon and sulfur in all forms. An additional 14 elements are measured after dilution in aqua regia. Prepared sample is digested with a modified aqua regia solution of equal parts concentrated HCl, $HNO_3$ and DI-$H_2O$ for one hour in a heating block or hot water bath. The sample is made up to volume with dilute HCl. Sample splits of 0.5 g are analyzed. None of the measured concentrations was too far above the possible detection (see Table 2) and accuracy and precision are between 2–3%.

### 2.6. Raman spectroscopy

Non-polarized micro-Raman spectra were obtained in nearly backscattered geometry with two different instruments and four different laser wavelengths at CNR-ICVBC Milano, University of Parma and University of Milano-Bicocca. The 632.8 nm line of a He–Ne laser and the 488 line of an Ar + laser were used for excitation with a Jobin-Yvon Horiba LabRam apparatus, equipped with an Olympus microscope with Å ~ 10, Å ~ 50 and Å ~ 100 objectives and a motorized x–y stage.

**Table 2**
Semi-quantitative estimation based on XRD peak relative intensities with annotation of existing minerals in decreasing abundances. Ant = anthophyllite; Trem = tremolite; Rieb = riebeckite; Chl = chlorite; Qz = quartz; Fd = feldspar.

| Locality | Sample | Minerals in decreasing abundances per sample | | | | | | | |
|---|---|---|---|---|---|---|---|---|---|
| Vindafjord | R6 | Talc | Clay | 14 Å | Qz | Fd | Hollandite | Pyrite | |
| Rennesøy | R12 | Talc | Chl | Qz | Clay | | | | |
| Hjelmeland | R9 | Talc | Trem | Ant | 14 Å | Qz | Clay | Chl | Fd |
| Hjelmeland | R10 | Talc | Ant | Clay | 14Å* | Qz | | | |
| Hjelmeland | R18 | Talc | Chl | Qz | Ant | Clay | Willemite | Litharge | |
| Klepp | R7 | Talc | Ant | Qz | Clay | Chl | Fd | | |
| Strand | R29 | Ant | Chl | Chl | Qz | Clay | | | |
| Gjesdal | R2 | Talc | Clay | Qz | 14 Å | Fd | Chl | | |
| Time | 11 | Talc | Qz | Ant** | Clay | Chl* | | | |
| Time | 12 | Talc | Chl | Clay | Rieb | Qz | | | |
| Hå | R14 | Talc | Qz | Clay | Chl | chrysotile | | | |
| Hå | R15 | Talc | Qz | Chl | Clay | Fd | | | |
| Hå | R31 | Talc | Chl | Trem | Qz | Clay | | | |

\* Broad XRD peaks.
\*\* Mg-Anthophyllite.

The system was calibrated using the 520.7 cm$^{-1}$ Raman silicon band before each experimental session. Spectra were generally collected with counting times ranging between 60 and 180 s. The 785 nm line of a NIR laser and the 532 nm line of a solid-state laser were used for excitation with a Bruker Senterra dispersive spectrometer, equipped with an Olympus microscope with Å ~ 20, Å ~ 50 and Å ~ 100 objectives and a motorized x–y stage. The system was automatically calibrated using the Raman frequencies of an internal neon lamp before each measurement. Spectra were collected with counting times ranging between 90 and 180 s. For both instruments, the minimum lateral and depth resolution was set to c. 2 mm with a confocal hole. Laser power was controlled by means of a series of density filters in order to avoid heating effects. The wavenumbers of the Raman bands were then determined by fitting with Voigt functions using the LabSpec software, after polynomial background removal. The uncertainty on the measured wavenumbers was estimated at less than 1 cm$^{-1}$, which allowed in identifying between mineralogical species even within isomorphous series (e.g. garnets, Bersani et al., 2009). Grains were individually selected for analysis, and time and focus have been set by the operator. At least three different spots were analyzed for each grain, and the best spectrum obtained was selected for identification.

## 3. Results

### 3.1. Mineralogy

Optical petrography could determine talc as the most abundant mineral, besides anthophyllite, which occurs elongated and orientated in a brownish matrix. The matrix is formed of organic matter and dark clay minerals and the minerals are often orientated along their c-axis (Fig. 3a). Talc is often curled and bend (Fig. 3b) and occurs mostly as a composite mineral, is strictly spoken a rock fragment (Fig. 3c) and can be relatively large, up to 500 μm. All other minerals are small (<70 μm) like few subangular quartz and alkalifeldspar as well as plagioclase (Fig. 3a). Rock fragments from felsic metasedimentary sources occur, but are rare. Epidote is also rare but appears euhedral as small grain (Fig. 3c). Further accessory minerals are corroded hornblende, actinolite, albite, rutile and almandine.

X-ray diffraction analyses show that most of the samples contain (Table 2) about 70–60% of different talcs (Mg and Ni-rich) as well as variable amounts of amphiboles (mainly Mg-rich anthophyllite and tremolite–actinolite) and chlorites (Mg and Ni-rich nimite) as dominant minerals, along with quartz, clay minerals, and traces of feldspars and other accessory minerals (Table 2). Three samples contain a 14 Å mineral, which could be a vermiculite or just chlorite after being heated over 450–550 °C, but there are no evident signs of firing at that temperature under FE-SEM observations to confirm its identification. Both, Mg- and Ni-rich talc willemseite ($(Ni, Mg)_3Si_4O_{10}(OH)_2$) were identified by XRD and FE-SEM–EDS. Another Cr-rich talc phase was determined with Raman spectroscopy. Chlorite can frequently be Ni-rich nimite ($(Ni, Mg, Al)_6(Si, Al)_4O_{10}(OH)_8$) but also a possible Cr-clinochlore, which has been identified in sample R9. In hydrous silicates such as phyllosilicates, Ni replacing Mg may occur over wide ranges of composition (Brindley and Maksimovic, 1974) so that there could be any intermediate mineral, not necessarily the end members of the series of talc-nimite. Sample 11 and R7 are somewhat different, as they do not show high amounts of talc, furthermore, R7 is dominated by anthophyllite (40–50%), 40% talc with subordinate quartz (Table 2).

Clay mineral assemblage has not been identified because of the small amount of sample available, but the broad peaks at 14 Å and at 4.56–4.50 Å suggest that they are present in significant proportions in samples R10, R12 and 12 and in lesser quantities in the other samples (Table 2).

The mineralogy varies with the site location of the samples. Differences in the mineral proportions and eventually their mineral composition are noticeable regarding the geographical site location. R9, R10 and R18 from Hjelmeland are asbestos-rich, containing tremolite (particularly R9, with c. 40%) and anthophyllite along with dominant talc, willemseite, a 14 Å mineral, minor clinochlore (and/or nimite), quartz and traces of plagioclase. R10 contains also traces of Zn and Pb bearing minerals such as willemite (2.89 Å reflection) and litharge, respectively. Willemite is a relatively common secondary zinc silicate in many Pb–Zn or Zn deposits, which contain or contained sphalerite, from which it is commonly formed upon oxidation in a siliceous environment and litharge is a secondary mineral, which forms from the oxidation of galena ores. R6 from Vindafjord is composed of talc, willemseite, a 14 Å mineral with quartz, scarce tremolite, and traces of hollandite and arsenopyrite. R2 from Gjesdal resembles the composition of R6. At Hå, R14, R15 and R31 are characterized by 60–70% of talc and willemseite, 20% clinochlore (and/or nimite), along with minor quartz and others (feldspars, clinochrysotile). Traces of chrysotile (asbestos of the serpentine group) have been identified based on its 7.45 Å peak in sample R14. R31 contains significant tremolite, while R29 from Strand, R12 from Rennesøy and 12 from Time are similar in minerals composition to this group, but the latter has riebeckite (confirmed by EDS) instead of tremolite. In contrast, sample 11, also from Time, has much lesser talc and willemseite but higher contents of quartz, Mg-anthophyllite with scarce chlorite and clay minerals. Finally, R7 from Klepp differs from all the other by the considerable larger and dominant amount of asbestos-like mineral anthophyllite and subordinate talc (and/or willemseite) as well as quartz (Table 2).
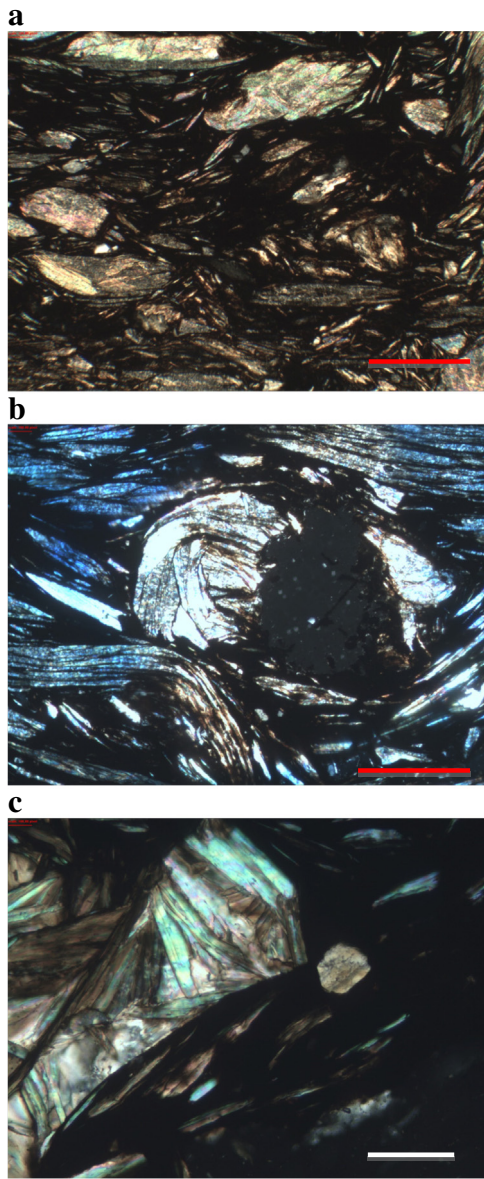
**Fig. 3.** Microphotograph of a sample of pottery from the Early Bucket shape pottery (Sample B5343 from Kvassheim, Hå, Rogaland). a) Overview in polarized light with the most abundant mineral talc in a dark brownish clay matrix; magnification 4×; scale: 100 μm; b) Talc minerals in different geometric forms (polarized light; magnification 10×; scale: 30 μm); c) Detail of a talc fragment (polarized light; magnification 10×; scale: 30 μm).

### 3.2. Field emission secondary electron microscope with energy dispersive system (FE-SEM-EDS)

The general textures of the samples are in most cases with strong phyllosilicate orientation surrounding usually rounded silty grains of quartz (occasionally feldspars and other accessory minerals) denoting the pressure applied during the manufacturing process (Fig. 4a). The grains are relatively loose as if they had not been subjected to high-temperature firing. The minerals identified by XRD where confirmed after FE-SEM–EDS observations, except for the Ni and Cr-rich phases. Talc-group minerals occurred in medium to large flat flakes (20–30 μm to 500 μm or even 1 mm) arranged in booklet-bundles (Fig. 4b), and frequently folded. Anthophyllite occurs in clusters of about 200 to 500 μm (Fig. 4c). Tremolite appears in slender prismatic crystals and rods of different lengths. The clay minerals can be found as very small flakes, sometimes smaller than 1 μm with $Mg^{2+}$ and $K^+$

as the main cations along with minor $Na^+$, $Ca^{2+}$ and Fe, suggesting a mixed-layer mineral with illite and possibly smectite since the flakes exhibit occasional crenulated ends (Fig. 4d). Significant amounts of fibrous organic material were found in R7 but also in lesser amounts in most pot fragments (Fig. 4e), well mixed within the sample, which might be dung. In R9, a very tiny rounded fragment of about 3 μm was observed and is interpreted as a silicon phytolith fragment.

### 3.3. Geochemistry

Generally, major element concentrations are relatively constant (with few important exceptions, see below; Table 3). No major or extraordinary variations exist within the oxides of Si, Al, Ti, Fe and Mn with very few exceptions (see below; Table 3). Some samples are slightly enriched in $P_2O_5$ compared to normal shale (PAAS; Post-Archean Australian Average Shale[1]), but strongly enriched in MgO. Hence, the samples are relatively depleted in nearly all other major elements compared to PAAS. R7 and 11 have the lowest values for $SiO_2$ and MgO, but the highest for $Na_2O$, $K_2O$, $TiO_2$ and $Al_2O_3$, which points to a different mineralogical composition. Some samples do contain high concentrations in selected elements like CaO (6.74 wt.% for R9) and $P_2O_5$ (0.79 wt.% for R9 and 1.06 wt.% for R29), which might be of post-manufacturing origin as typical carbonate (calcite, dolomite) and phosphate (apatite, monazite) minerals have not been detected with the applied methods. TOT/C varies between 1.06 and 3.73 wt.% but is the highest in R7 (1.39%) and 11 (5.46%) and does not correlate with CaO, hence does not reflect carbonate phases, rather organic matter.

Using trace element geochemistry allows in interpreting the general overall composition of the used geological materials and may be able in determining their origins (e.g. McLennan et al., 1990). Major elements are mostly mobile, besides $SiO_2$, $Al_2O_3$ and $TiO_2$ and therefore prone to a variety of secondary effects like fluid-flow, weathering, diffusion etc. (e.g. Taylor and McLennan, 1985) and may be strongly affected during the manufacturing process of pottery and therefore not used here. Ratios of Zr/Ti versus Nb/Y will reflect the general geochemical composition (Fralick, 2003; Winchester and Floyd, 1977). All samples show relatively narrow variations in Nb/Y (0.51 to 0.86) and Zr/Ti ratios. However, the occurring small variation in both ratios might point to the partly use of slightly more alkaline material to increase Nb over Y and in some samples a slight dominance of felsic material with values above 0.04 (R2, R7, R14, R15 and R31; Table 3; Fig. 5a) or a dominance of less fractionated rock components with values below 0.04 (samples R6, R9, R10, R12, R18, 11, 12, Table 3). However, Ti is nearly 100% budgeted by rutile but not all mafic to ultramafic rocks do contain rutile to increase Ti concentrations, but it can also be originated in metamorphic rocks. A similar trend of two slightly differently mixed source components can be observed when using Th/Sc versus Zr/Sc ratios (Table 2; Fig. 5b; McLennan et al., 1990, 1993), which may divide the samples in two groups. Here samples like 11 does show clearly the input of felsic material with elevated Zr concentrations (second highest) in comparison to other samples and the significant Sc concentrations still point to the use of a non-felsic component (Table 3). High sensitive rare earth elements (REE) are able to determine the main component and may reveal differences in rock compositions. However, the sum of REE (ΣREE) is very low in comparison to normal PAAS (ΣREE = 183 ppm; after McLennan et al., 2006) with values between 37.6 and 116 ppm (Table 3) in all samples but the patterns are relatively similar to normal shales (Fig. 5c). Some samples do show a significant negative Eu anomaly (e.g., R31), while other samples are characterized by a flat pattern
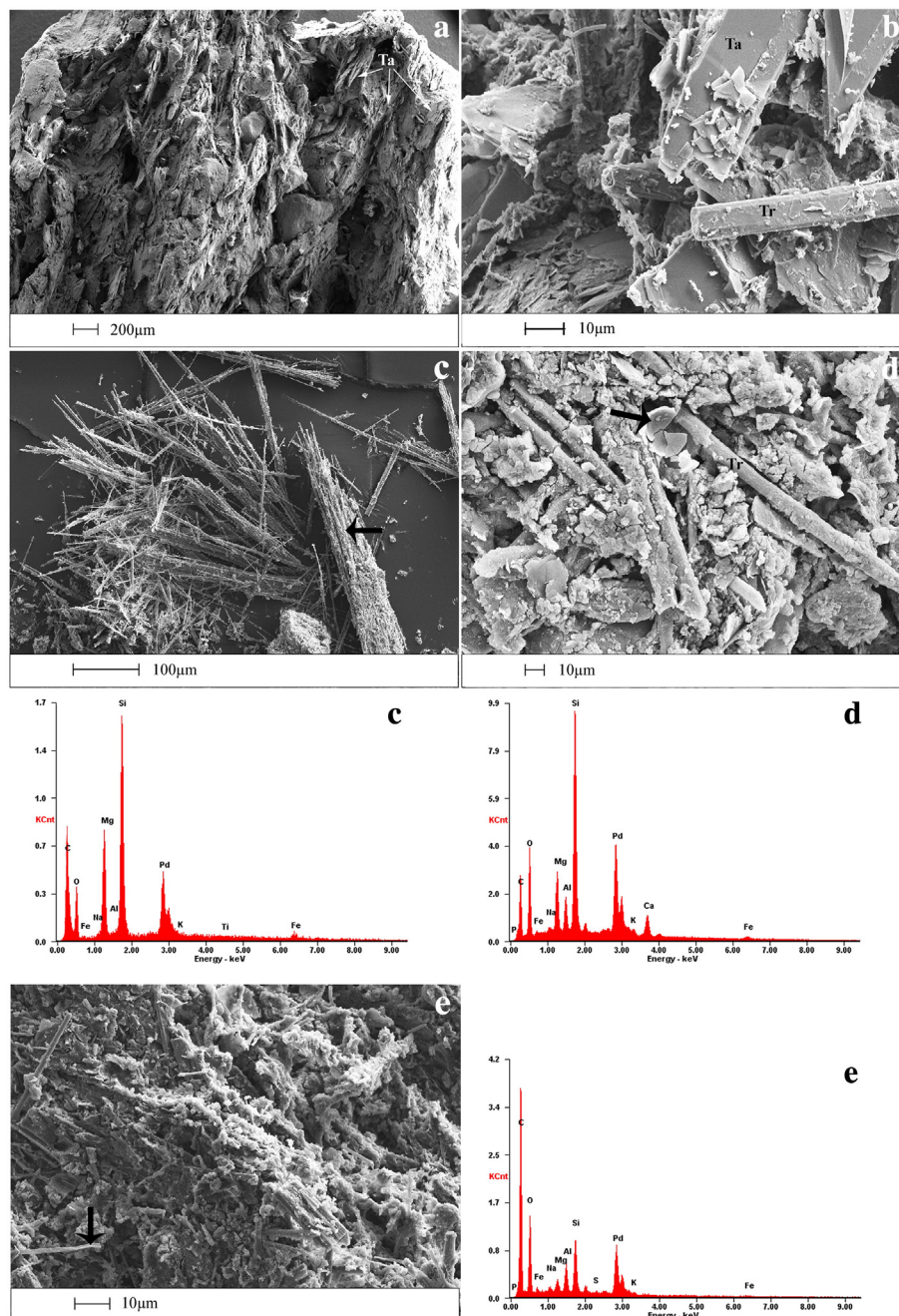
Fig. 4. Selected FE-SEM micrographs and EDS of the studied samples. Note the loose arrangement of particles. a) R14, general texture of the paste, strong orientation of talc booklets (Ta) and other minerals surrounding rounded quartz and silty grains; b) R31, talc (Ta) flat flakes and booklets and tremolite (Tr) prismatic crystals; c) R7, large bunches of anthophillite (arrow), EDS spectra c shows its chemical composition; d) R9, long prismatic crystals of tremolite, aggregates of small clay particles, talc flat flakes, the rounded fragment (arrow) has high concentration of Si (other elements might be contamination from the small clay particles) as shown in the EDS spectra d and suggests a silicious phytolith; e) R7, observed the abundance of long tubes (arrow) of organic matter mixed in the paste, EDS e shows high C concentration.

(e.g., 11 and R7; Fig. 5c). Other samples (e.g., R14) are depleted in REE and show high concentrations in heavy REE and lower abundances of light REE. Normalizing a larger variety of large ion lithophile elements (LILE; K, Ba, Cs, Rb, Sr), high field strength elements (HFSE; Zr, Hf, Nb, U) and first series transition metals (Sc, Ti, V, Cr, Ni) to typical shale composite (PAS after Taylor and McLennan, 1985; McLennan, 2001; McLennan et al., 2006; Fig. 5d) should be able to reveal anomalies of specific element groups, like f.e. compatible elements (Sc, Ti, Ni, Cr, V, Nb), which would point to a mafic or ultra-mafic source, in contrast to incompatible trace element indicating a felsic source component (Th, La, Ce, Zr, Hf). Mobile elements like the LILE are, in the presented samples, depleted in comparison to PAS, with the exception of P. However,

P is relatively mobile and could be also of anthropogenic origin introduced via fertilizer in those samples, where it is enriched. This is likely as other incompatible elements are depleted to normal shale (Fig. 5d). Most of the immobile elements are also depleted compared to normal shale similar to the LILE, but not Cr, Ni and Co (Table 3). Cr and Ni are strongly enriched in all samples but not in 11 and R7 (Fig. 5d). This directs to specific mineral phases, enriched in these two compatible elements, as being abundant in the pottery material. Other compatible elements, like Nb, Ta, Ti and Sc are depleted or as abundant as in normal shale (Fig. 5d; Table 3). Generally, it is impressive how similar the concentrations in these selected elements are in these selected elements, which is indicated by the gray area (Fig. 5d). It seems that all samples

ARTICLE IN PRESS

**Table 3**

Geochemical data for all samples used in this study. % = weight percent. ppm = parts per million; ppb = parts per billion; TOT/C = total Carbon; TOT/S = total sulfur; LOI = loss on ignition; n.d. = not determined; bdl = below detection limit. Values for PAAS (Post-Archean Australian average shale) are from McLennan (2001) and McLennan et al. (2006) completed with values for the upper continental crust (UCC) by Rudnick and Gao (2003) because those elements have not been compiled in the former literature and reliable data for PAAS for these elements are not available. Data from rocks of Karmøy are taken from Pedersen and Hertogen (1990).

| Element | | SiO$_2$ | Al$_2$O$_3$ | Fe$_2$O$_3$ | MgO | CaO | Na$_2$O | K$_2$O | TiO$_2$ | P$_2$O$_5$ | MnO | LOI | Sum | Ba | Cs | Ga | Hf | Nb | Rb | Sr | Ta |
|---|---|---|---|---|---|---|---|---|---|---|---|---|---|---|---|---|---|---|---|---|---|
| Unit | | % | % | % | % | % | % | % | % | % | % | % | % | ppm | ppm | ppm | ppm | ppm | ppm | ppm | ppm |
| Sample | Type | | | | | | | | | | | | | | | | | | | | |
| Detection limit | | 0.01 | 0.01 | 0.04 | 0.01 | 0.01 | 0.01 | 0.01 | 0.01 | 0.01 | 0.01 | 0.1 | 0.01 | 1 | 0.1 | 0.5 | 0.1 | 0.1 | 0.1 | 0.5 | 0.1 |
| Upper limit | | 100% | 100% | 100% | 100% | 100% | 100% | 100% | 100% | 100% | 100% | 100% | 100% | 5% | 10000 | 10000 | 10000 | 10000 | 10000 | 50000 | 10000 |
| R2 | Grave | 58.05 | 5.65 | 5.54 | 17.67 | 0.48 | 0.42 | 0.98 | 0.28 | 0.28 | 0.08 | 9.9 | 99.65 | 218 | 1.7 | 6.8 | 2.2 | 6.1 | 46.8 | 50.1 | 0.6 |
| R6 | Grave | 53.17 | 6.68 | 6.66 | 20.78 | 0.91 | 0.41 | 0.65 | 0.25 | 0.33 | 0.1 | 9.3 | 99.61 | 113 | 2.8 | 9.7 | 1.4 | 4.4 | 33.9 | 34 | 0.4 |
| R7 | Grave | 45.05 | 7.61 | 5.61 | 10.85 | 0.91 | 0.95 | 1.56 | 0.44 | 1 | 0.1 | 25.6 | 99.69 | 467 | 3.2 | 11.3 | 3.4 | 9.9 | 69.9 | 142.3 | 0.7 |
| R9 | Grave | 52.78 | 5.58 | 5.56 | 16.52 | 6.74 | 0.28 | 0.99 | 0.29 | 0.76 | 0.13 | 9.8 | 99.68 | 200 | 3.1 | 8.2 | 1.5 | 6 | 55.5 | 41.1 | 0.6 |
| R10 | Grave | 50.03 | 5.26 | 8.02 | 20.84 | 0.86 | 0.24 | 0.59 | 0.24 | 0.2 | 0.16 | 12.4 | 99.26 | 119 | 1.9 | 10.1 | 1.1 | 6.6 | 28.1 | 32.8 | 0.5 |
| R12 | Grave | 52.8 | 5.66 | 7.09 | 22.07 | 0.26 | 0.26 | 0.88 | 0.41 | 0.49 | 0.06 | 9.3 | 99.58 | 151 | 1.5 | 9.6 | 2.4 | 7.1 | 34 | 26 | 0.5 |
| R14 | Grave | 59.08 | 5.71 | 5.64 | 19.21 | 0.43 | 0.4 | 0.83 | 0.28 | 0.08 | 0.08 | 7.6 | 99.65 | 123 | 1.6 | 6.8 | 2.5 | 6.2 | 32.7 | 34.5 | 0.7 |
| R15 | Grave | 58.78 | 6.43 | 5.66 | 18.32 | 0.45 | 0.42 | 0.95 | 0.31 | 0.31 | 0.08 | 7.6 | 99.61 | 151 | 1.6 | 7.1 | 2.4 | 5.6 | 37.2 | 37.8 | 0.5 |
| R18 | Grave | 53.61 | 5.28 | 7.88 | 20.94 | 1.19 | 0.21 | 0.83 | 0.32 | 0.42 | 0.15 | 8.5 | 99.6 | 112 | 1.8 | 8.4 | 1.9 | 7.3 | 31.6 | 27.5 | 0.6 |
| R29 | Grave | 50.42 | 6.13 | 6.89 | 20.19 | 0.26 | 0.41 | 0.91 | 0.29 | 1.06 | 0.04 | 12.5 | 99.58 | 231 | 1.7 | 10.9 | 1.1 | 6.8 | 53.9 | 51.3 | 0.5 |
| R31 | House-pottery | 55.14 | 4.22 | 5.9 | 23.05 | 1.13 | 0.34 | 0.62 | 0.16 | 0.47 | 0.04 | 8.2 | 99.58 | 132 | 1.1 | 7.2 | 1.4 | 3.9 | 31 | 36 | 0.2 |
| 11 | Grave | 52.05 | 8.65 | 6.92 | 14.85 | 0.68 | 0.68 | 1.71 | 0.37 | 0.46 | 0.12 | 12.9 | 99.41 | 253 | 3.9 | 10.8 | 2.4 | 7.6 | 86.3 | 59.6 | 0.5 |
| 12 | Grave | 51.94 | 7.72 | 7.2 | 19.37 | 1.26 | 0.3 | 0.91 | 0.33 | 0.38 | 0.1 | 9.8 | 99.62 | 152 | 2.5 | 10.8 | 2 | 6.9 | 45.2 | 26.3 | 0.5 |
| PAAS and UCC | | 62.80 | 18.90 | 6.50 | 2.20 | 1.30 | 1.20 | 3.70 | 1.00 | 0.16 | 0.11 | | | 650 | 15.0 | 20 | 5 | 19.0 | 160 | 200 | 1 |
| Possible sources | | | | | | | | | | | | | | | | | | | | | |
| Karmøy | Gabbro | | | | 8.53 | | | | 0.31 | | | | | | | | | 0.22 | | | 0.04 |
| Karmøy | Gabbro | | | | 9.68 | | | | 0.47 | | | | | | | | | 0.14 | | | 0.02 |
| Karmøy | Dyke swarm | | | | 17.32 | | | | 0.19 | | | | | | | | | n.d. | | | 0.04 |
| Karmøy | Dyke swarm | | | | 13.7 | | | | 0.34 | | | | | | | | | n.d. | | | 0.04 |

**Table 3** (*continued*)

| Element | | Co | Cr | Ni | Sc | Th | U | V | Zr | Y | La | Ce | Pr | Nd | Sm | Eu | Gd | Tb | Dy | Ho | Er |
|---|---|---|---|---|---|---|---|---|---|---|---|---|---|---|---|---|---|---|---|---|---|
| Unit | | ppm | ppm | ppm | ppm | ppm | ppm | ppm | ppm | ppm | ppm | ppm | ppm | ppm | ppm | ppm | ppm | ppm | ppm | ppm | ppm |
| Sample | Type | | | | | | | | | | | | | | | | | | | | |
| Detection limit | | 0.2 | 5 | 0.1 | 1 | 0.2 | 0.1 | 8 | 0.1 | 0.1 | 0.1 | 0.1 | 0.02 | 0.3 | 0.05 | 0.02 | 0.05 | 0.01 | 0.05 | 0.02 | 0.03 |
| Upper limit | | 10000 | 1 | 10000 | 10000 | 10000 | 10000 | 10000 | 50000 | 50000 | 50000 | 50000 | 10000 | 10000 | 10000 | 10000 | 10000 | 10000 | 10000 | 10000 | 10000 |
| R2 | Grave | 42.5 | 1539 | 120 | 7 | 4.6 | 0.9 | 48 | 77 | 9.9 | 11.7 | 24.9 | 2.87 | 10.1 | 1.99 | 0.37 | 1.78 | 0.29 | 1.67 | 0.34 | 1 |
| R6 | Grave | 51.2 | 1628 | 439.4 | 10 | 4.9 | 0.8 | 88 | 44.6 | 7.9 | 8.9 | 23.4 | 2.38 | 9.8 | 1.91 | 0.37 | 1.46 | 0.25 | 1.4 | 0.27 | 0.84 |
| R7 | Grave | 18.3 | 246 | 48 | 10 | 7.7 | 3.4 | 74 | 125.3 | 14.8 | 24.3 | 50.9 | 5.64 | 21.1 | 3.47 | 0.66 | 2.86 | 0.44 | 2.49 | 0.53 | 1.49 |
| R9 | Grave | 36.6 | 978 | 397.4 | 9 | 5.7 | 1 | 50 | 52.5 | 11.7 | 12.1 | 27.9 | 3.12 | 11.5 | 2.46 | 0.37 | 2.24 | 0.38 | 2.2 | 0.44 | 1.25 |
| R10 | Grave | 58.6 | 2456 | 109 | 9 | 4.8 | 1.8 | 63 | 47.9 | 10.6 | 16.4 | 33.9 | 3.61 | 12.4 | 2.31 | 0.38 | 1.89 | 0.31 | 1.66 | 0.34 | 1.03 |
| R12 | Grave | 40.7 | 1143 | 133.8 | 9 | 6.4 | 1.2 | 70 | 80.4 | 11.4 | 14.5 | 30.6 | 3.59 | 13.6 | 2.4 | 0.32 | 2.15 | 0.33 | 1.96 | 0.4 | 1.22 |
| R14 | Grave | 41.5 | 1081 | 121.5 | 6 | 3.8 | 0.6 | 44 | 77.5 | 7.2 | 6.4 | 1.3 | 1.69 | 6 | 1.3 | 0.25 | 1.07 | 0.2 | 1.21 | 0.24 | 0.8 |
| R15 | Grave | 43.6 | 1245 | 129.8 | 7 | 4.5 | 1 | 44 | 84.2 | 8.1 | 9.4 | 25.2 | 2.51 | 8.9 | 1.86 | 0.34 | 1.52 | 0.26 | 1.5 | 0.3 | 0.95 |
| R18 | Grave | 51.9 | 1232 | 222.3 | 11 | 5.4 | 1.6 | 52 | 68.6 | 10.5 | 15.2 | 29.9 | 3.39 | 13 | 2.36 | 0.36 | 2.06 | 0.35 | 1.97 | 0.37 | 1.14 |
| R29 | Grave | 48.7 | 2750 | 106.3 | 9 | 7 | 1.5 | 60 | 40 | 9 | 20.5 | 43.8 | 4.76 | 17.1 | 2.93 | 0.44 | 2.2 | 0.32 | 1.71 | 0.28 | 0.83 |
| R31 | House-pottery | 15.8 | 1697 | 88.6 | 4 | 5.7 | 1.2 | 37 | 43.3 | 7.3 | 14.2 | 33.3 | 3.38 | 11.4 | 2.31 | 0.3 | 1.74 | 0.27 | 1.44 | 0.24 | 0.64 |
| 11 | Grave | 30.2 | 123 | 51.6 | 9 | 8 | 1.4 | 65 | 85.7 | 11.7 | 19.3 | 39.9 | 4.42 | 17.2 | 2.89 | 0.56 | 2.4 | 0.39 | 2.03 | 0.43 | 1.23 |
| 12 | Grave | 51.8 | 1539 | 128.5 | 16 | 6.2 | 1.3 | 77 | 61.2 | 11.3 | 14 | 31.8 | 3.36 | 13.5 | 2.31 | 0.37 | 1.98 | 0.36 | 1.98 | 0.4 | 1.25 |
| PAAS and UCC | | 23.0 | 110 | 55 | 16.0 | 14.6 | 3.1 | 150 | 210 | 27.0 | 38.0 | 80.0 | 8.9 | 32.0 | 5.6 | 1.1 | 4.7 | 0.8 | 4.4 | 1.0 | 2.9 |
| Possible sources | | | | | | | | | | | | | | | | | | | | | |
| Karmøy | Gabbro | n.d. | 808 | 210 | 37.3 | 0.06 | | 94 | 27 | 5.8 | | | | | | | | | | | |
| Karmøy | Gabbro | n.d. | 611 | 148 | 39.6 | 0.05 | | 132 | 26 | 10.3 | | | | | | | | | | | |
| Karmøy | Dyke swarm | n.d. | 1351 | 271 | 42.1 | 0.2 | | 199 | 16 | 6 | | | | | | | | | | | |
| Karmøy | Dyke swarm | n.d. | 1277 | 177 | 36.8 | 0.25 | | 190 | 14 | 12 | | | | | | | | | | | |

**Table 3** (continued)

| Sample | Type | ΣREE | Lu | Yb | Tm | TOT/C | TOT/S | Mo | Cu | Pb | Zn | As | Cd | Au | Ag | Zr/Ti | Nb/Y | Th/Sc | Zr/Sc | Cr/V | Cr/Th | Y/Ni |
|---|---|---|---|---|---|---|---|---|---|---|---|---|---|---|---|---|---|---|---|---|---|---|
| Element | | | | | | | | | | | | | | | | | | | | | | |
| Unit | | ppm | ppm | ppm | ppm | % | % | ppm | ppm | ppm | ppm | ppm | ppm | ppb | ppm | | | | | | | |
| Detection limit | | | 0.01 | 0.05 | 0.01 | 0.02 | 0.02 | 0.1 | 0.1 | 0.1 | 1 | 0.5 | 0.1 | 0.5 | 0.1 | | | | | | | |
| Upper limit | | | 10000 | 10000 | 10000 | 100% | 100% | 2000 | 10000 | 10000 | 10000 | 10000 | 2000 | 100000 | 100 | | | | | | | |
| R2 | Grave | 58.35 | 0.15 | 1.02 | 0.17 | 3.31 | 0.03 | 0.1 | 23.1 | 6.6 | 30 | 1.6 | 0.2 | 2.6 | bdl | 0.046 | 0.62 | 0.66 | 11.00 | 32 | 335 | 0.08 |
| R6 | Grave | 52 | 0.12 | 0.78 | 0.12 | 1.06 | 0.05 | 0.2 | 53.3 | 9.1 | 67 | 97.8 | bdl | bdl | 0.1 | 0.030 | 0.56 | 0.49 | 4.46 | 19 | 332 | 0.02 |
| R7 | Grave | 115.82 | 0.21 | 1.5 | 0.23 | 13.39 | 0.08 | 4.2 | 119.4 | 16.7 | 50 | 2.5 | 0.5 | 3.2 | 1.0 | 0.048 | 0.67 | 0.77 | 12.53 | 3 | 32 | 0.31 |
| R9 | Grave | 65.44 | 0.16 | 1.14 | 0.18 | 2.35 | 0.02 | 0.3 | 32.4 | 17 | 51 | 1.7 | bdl | 6.0 | bdl | 0.030 | 0.51 | 0.63 | 5.83 | 20 | 172 | 0.03 |
| R10 | Grave | 75.52 | 0.15 | 0.98 | 0.16 | 3.33 | 0.18 | 0.2 | 8.7 | 40.5 | 3202 | 9 | 3.6 | 1.5 | bdl | 0.033 | 0.62 | 0.53 | 5.32 | 39 | 512 | 0.10 |
| R12 | Grave | 72.67 | 0.19 | 1.21 | 0.2 | 2.04 | 0.02 | 0.3 | 17.2 | 8.3 | 47 | 4 | bdl | 4.2 | bdl | 0.033 | 0.62 | 0.71 | 8.93 | 16 | 179 | 0.09 |
| R14 | Grave | 37.64 | 0.13 | 0.83 | 0.13 | 1.16 | bdl | 0.2 | 14.5 | 6.9 | 32 | 1 | bdl | 2.2 | 0.1 | 0.046 | 0.86 | 0.63 | 12.92 | 25 | 284 | 0.06 |
| R15 | Grave | 53.91 | 0.17 | 0.9 | 0.14 | 1.14 | 0.02 | 0.5 | 179.4 | 9.7 | 112 | 1.2 | bdl | 1.5 | bdl | 0.045 | 0.69 | 0.64 | 12.03 | 28 | 277 | 0.06 |
| R18 | Grave | 71.55 | 0.1 | 1.11 | 0.17 | 1.51 | bdl | 0.3 | 12.3 | 12.4 | 42 | 56.9 | bdl | 12.7 | 0.2 | 0.036 | 0.70 | 0.49 | 6.24 | 24 | 228 | 0.05 |
| R29 | Grave | 95.81 | 0.08 | 0.73 | 0.11 | 3.73 | 0.02 | 0.3 | 125.1 | 15.7 | 44 | 38.2 | 0.1 | 13.8 | 6.7 | 0.023 | 0.76 | 0.78 | 4.44 | 46 | 393 | 0.08 |
| R31 | House-pottery | 70.09 | 0.17 | 0.69 | 0.1 | 1.62 | bdl | 0.3 | 20.1 | 4.6 | 13 | 18.4 | bdl | 3.5 | bdl | 0.045 | 0.53 | 1.43 | 10.83 | 46 | 298 | 0.08 |
| 11 | Grave | 92.25 | 0.16 | 1.15 | 0.18 | 5.46 | bdl | 0.2 | 1924.2 | 231.6 | 46 | 4.2 | 0.1 | 2.2 | 0.6 | 0.039 | 0.65 | 0.89 | 9.52 | 2 | 15 | 0.23 |
| 12 | Grave | 72.8 | | 1.16 | 0.17 | 2.22 | bdl | 0.4 | 8.5 | 9.1 | 44 | 2.1 | bdl | bdl | bdl | 0.031 | 0.61 | 0.39 | 3.83 | 20 | 248 | 0.09 |
| PAAS and UCC | | 183 | 0.43 | 2.8 | 0.40 | | 0.621 | 1.0 | 50 | 20 | 85 | 4.8 | 0.09 | 1.5 | 0.056 | 0.035 | 0.70 | 0.91 | 13.13 | 1 | 8 | 0.49 |
| Possible sources | | | | | | | | | | | | | | | | | | | | | | |
| Karmøy | Gabbro | | | | | | | | | | | | | | | 0.015 | 0.04 | 0.002 | 0.72 | 9 | 13467 | 0.03 |
| Karmøy | Gabbro | | | | | | | | | | | | | | | 0.009 | 0.01 | 0.001 | 0.66 | 5 | 12220 | 0.07 |
| Karmøy | Dyke swarm | | | | | | | | | | | | | | | 0.014 | | 0.005 | 0.38 | 7 | 6755 | 0.02 |
| Karmøy | Dyke swarm | | | | | | | | | | | | | | | 0.007 | | 0.007 | 0.38 | 7 | 5108 | 0.07 |

do follow a relatively similar composition in the selection of the material used for the pottery besides 11 and R7.

Mafic and ultramafic rocks are enriched in compatible elements, however different tectonic settings would produce different types of mafic and ultramafic rocks. Indicator for a mafic to ultramafic composition or a dominant mafic to ultramafic component in clastic material can be monitored with Cr/Th (Fig. 5e) and Cr/V ratios (Fig. 5f). The samples studied here have Cr/V ratios up to 46 (!) even higher than the compared primitive basalts and ultramafic rocks from Karmøy (Fig. 5f; Table 3). Basalts do have as well often elevated Cr/V ratios but they differ in Cr/Th ratios in comparison to ultramafic rocks (Floyd et al., 1990). Ultramafic rocks would show ratios far above 5000 while basaltic rocks rarely above 5, and post Archean average shale would have values around 7.5 (McLennan et al., 2006). Again all samples besides R7 and 11 point to an ultramafic source for the used pottery material, representing the less fractionated component of the used materials. Regarding Cr/V ratios, a value above 8 would point to an ophiolite of mafic to ultramafic composition that indicates a source represented by obducted oceanic or back-arc crust. Those rocks are as well enriched in ferromagnesium minerals, hence enriched in Ni but depleted in V with therefore low Y/Ni ratios (Fig. 5f; McLennan et al., 1993). The samples in this study do exactly show these characteristics, with the exception of samples R7 and 11 (Table 3).

Besides the spectacular concentrations of Cr (>1000 ppm) and Ni (100–5000 ppm), some other trace element concentrations are noteworthy. Cu, for example is enriched in sample R15 (but not in sample R14 from the same area), R29 and R7, but extremely abundant in sample 11 with nearly 2 wt.% (Table 3). This sample also is enriched in Pb with 10× normal shale (Table 3). Zn is in all samples depleted besides a slight enrichment in sample R15 but as abundant as 3 wt.% (!) in R10 (Table 3). Arsenic is in some samples strongly depleted but enriched in R29, R18, R31 and especially in R6 abundant. In rock and sediment samples base metals are rarely enriched mostly only if the rocks have been deposited under anoxic conditions or if they suffered from mineralizations (Piper, 1993). Cadmium concentration in sample R7 and R10 is wide above what to expect in rocks but can be possible in stream sediments where placer does enrich the material (Callender, 2003). Finally, Au is very slightly enriched in most of the samples, but R29 and R15 do show enrichment of about 10 times the typical value for crustal rocks (Table 3). R29 is also enriched in Ag for about 100 times compared to upper crustal rocks.

### 3.4. Raman spectroscopy

Raman spectroscopy is able to identify without damaging the material crystalline structures and therefore minerals (e.g., Andò and Garzanti, 2013; Fig. 6) have been identified with a wide range of expected and common minerals, like quartz, plagioclase (Fig. 6c) and biotite. Abundant, but mainly as small black entity, a black material is present in all the samples and the Raman spectra show amorphous carbon (coal; Fig. 6d). However, we cannot exclude that in origin this material was an organic substance subsequently transformed in carbonaceous material or has other origins. Of importance is the most abundant mineral identified as platy transparent crystals. Those minerals belong to the talc-group, as revealed by the spectra in both low-frequency (100–1200 $cm^{-1}$) and OH-stretching (3400–3800 $cm^{-1}$) regions (Fig. 6a). Furthermore, many prismatic and fibrous amphiboles exist, which appear as colorless or pale yellow crystals and are identified as anthophyllite (in the low frequency region with the laser polarization parallel and perpendicular to the elongation (c) axis of the crystals and also in the OH-stretching region; Fig. 6b). Of highest importance for this study was the discovery that most of the talc is enriched in Cr (Cr-rich talc; Fig. 6e), which is the main carrier of the high Cr concentration in the samples. No other Cr-bearing mineral has been so far discovered.
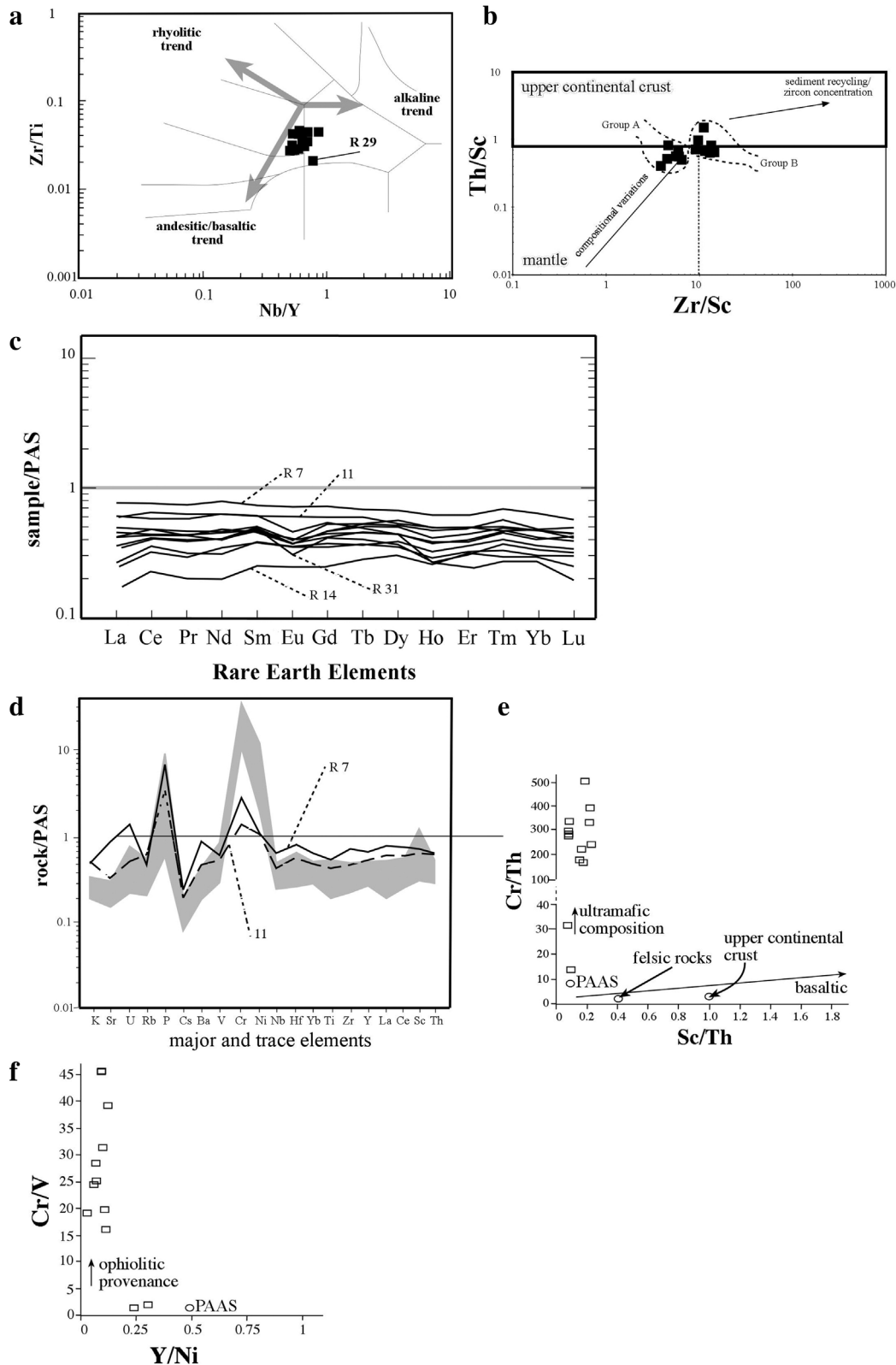
Fig. 5. a) General chemical composition of the pottery samples using Nb/Y and Zr/Ti ratios after Winchester and Floyd (1977); b) Zr/Sc versus Th/Sc for further details on the chemical composition of the samples. One group contains less fractionated material than other samples, although differences are minute; c) Rare earth element values normalized to normal shale (PAAS, McLennan, 2001; Taylor and McLennan, 1985); d) Values for the studied samples used in a multi-element diagram normalized to PAS (McLennan, 2001; Taylor and McLennan, 1985) and upper crust (Rudnick and Gao, 2003). The gray area envelopes all samples, but R7 and 11, and points to a narrow range for all elements, mobile and immobile ones; e) Ultramafic composition in clastic material would be identified with values between 30 to 50 (after Floyd and Leveridge, 1987), higher values like here are only one dimension below possible source rocks and extreme high (see Tables 3, 4); f) An ophiolitic (mafic to ultramafic) provenance starts in clastic material at a Cr/V ratio around 8 and reaches values of 12 possibly 15 (after McLennan et al., 1993) but in these samples much higher.

# 4. Implications of the analytical data

XRD, optical petrography together with Raman spectroscopy (Figs. 3, 5, 6; Table 1) determined a domination of Cr-rich and Ni-rich talc (willemseite) and chlorite (nimite), besides the 14 Å mineral and anthophyllite in the pottery explaining the high Cr and Ni abundances revealed by trace element chemistry. However, the most abundant mineral is Cr-bearing talc (Fig. 6e). Quartz and feldspar are rare, so are rock fragments and mica. The accessory mineral assemblage points rather to a preference for intermediate and mafic material components for the pottery with minerals like plagioclase, hornblende and rutile. Few minerals as the mentioned quartz, feldspar and epidote might be related to weathered felsic rocks (granites). Cr- and Ni-bearing talc is the most abundant phase with c. 40–60% (f.e. Table 2) dependent on the samples, and amounts for the high concentrations of Ni and Cr in the pottery. Anthophyllite, which is also abundant in the pottery (Table 2), is a Mg-Fe-Mn rich amphibole and is classified as an asbestos mineral (Veblen, 1980). Tremolite is sometimes present in asbestos-like long slender prismatic crystals but more often crushed in small rods or prismatic fragments. The occurrence of this mineral might have been decisive in the description of 'asbestos-bearing pottery' for the Bucket-shape ceramic of Rogaland (Kleppe and Simonsen, 1983). However, talc is by far more abundant in the pottery than anthophyllite (Table 2).

For the issue of the provenance and to explain the extraordinary chemical composition, the four mainly occurring minerals Cr-rich talc, willemseite, nimite and anthophyllite are decisive. All four are related to weathered ultramafic or mafic rocks (Bucher and Grapes, 2011; De Waal, 1970; Hora, 1997; Villanova-de-Benavent et al., 2014), which is supported by the geochemical data. Studies of Bronze Age and Roman Pottery from Cyprus showed the same trend and were related to the exposed ophiolite sequence of Troodos (Gomez et al., 2002). The high concentrations of Mg but low abundances of Al (Table 3) in our study can also be explained by the massive abundance of talc-group minerals. Further carriers of Mg are some clays, the 14 Å mineral (mica) and Mg-anthophyllite (amphibole group mineral). Trace element geochemistry could identify a composition, which is dominated by materials derived from ultramafic to mafic rocks with very high Cr/V (>10) and Cr/Th (>80) ratios and mixed with moderately recycled intermediate to possible felsic components (Fig. 5e and f; Table 4). Exceptions to all these generals are the samples R7 and 11. Both do not show the high amount of Cr, Ni and Co but still carry outstanding concentrations (Table 3). Sample 11 contains nearly 2 wt.% of Cu and more than 200 ppm Pb, while sample R7 has a high concentration of volatiles and TOC (Table 2). Both have been collected relatively close to each other and further sampling has to focus if this is a local variation or arbitrary.

Combining these information it is possible to suggest several major source areas for the origin of the used materials. The high amount of Mg, Cr, Ni and Co points to a mafic to ultramafic source for the materials, which is not related to a continental arc but to oceanic or back-arc crust. Mafic and ultramafic rocks related to oceanic crust and back-arc environments are enriched in ferromagnesium minerals (McLennan et al., 1990) and depleted in elements like Ti, Nb and Ta (Hofmann, 1988). Exactly this trend can be observed here (Table 3). To determine the type of origin for this mafic to ultramafic component is difficult as especially ultramafic rocks are highly variable and contain complex geochemistry (e.g. Zhou et al., 2004). However, rocks of that origin are exposed in Rogaland to the north of Stavanger on the island Karmøy (stippled area in Fig. 1) and belong to the Paleozoic Caledonian orogen. Sedimentary rocks with detritus derived from mafic and ultramafic rocks have been found in this orogen, hence are abundant and possible to identify (Floyd et al., 1989, 1991). On Karmøy, oceanic back-arc mafic and ultramafic rocks are exposed (Dilek and Furnes, 2011; Pedersen and Hertogen, 1990) and a good fit for the observed geochemical characteristics as even some rock successions exposed in the Karmøy ophiolite resemble the chemical composition of the pottery (Table 3). The higher

Cr/Th ratios are related to extreme depletion of Th in the mantle sources for these ophiolitic rocks and the lower Cr/V ratios are related to the major source of V in mafic and ultramafic rocks, which are spinels (Taylor and McLennan, 1985) and prone to sorting during weathering processes. As mafic, and especially ultramafic rocks are easily affected by weathering, secondary materials as a weathering product of possible different ages should be abundant on Karmøy. No other area in southern Norway contains a similar rock association and would produce such composed derivate usable for pottery production. Ophiolites exposed further north of Bergen are geochemically different and have a different origin and would not match the results here (Furnes et al., 1982). Cr and Ni concentrations at Storøya (Leka Ophiolite Complex close to Trondheim) are by far lower than in the rocks of Karmøy (Tveit et al., 1993). As remarked, a very similar relation between pottery composition and source rock composition with a mafic to ultramafic signature has been reported by Gomez et al. (2002) from Cyprus, where half of the island is composed of obducted oceanic crust, the world-famous Troodos massif (Dilek and Furnes, 2011).

Furthermore, alteration products of mafic and ultramafic rocks are enriched in the few slightly more stable minerals like amphiboles and spinels. The lack of the latter can be explained by sorting, as during heavy rainfall these minerals will be leached out easier from sediments than the strongly adhesive phyllosilicates or, alternatively, the pottery material used had been devoid of any other mafic minerals. The abundance of talc can be explained by weathering of intrusive contacts between silicate-poor and intermediate rocks in numerous locations on Karmøy where dykes intrude intermediate, mafic and ultramafic rocks (Pedersen and Hertogen, 1990). Geochemical studies on mafic and ultramafic rocks and dykes on Karmøy support our provenance speculations as rocks with Cr concentrations above 1000 ppm and Ni concentrations over 150 ppm are often recorded (Pedersen and Hertogen, 1990; Table 3). The area on Karmøy and especially around the Cu mines near Kopervik could also explain the extreme high abundances of Zn and Cu in some samples (Table 3). However, the latter is speculative as these concentrations can also be of anthropogenic origin.

This leaves us with the other, less significant material components, which are by far more difficult to pinpoint. Here, Table 3 and Fig. 5 show that samples are partly enriched in Th but depleted in Zr. This points rather to an intermediate component possibly deposited in an arc environment when this component would also be responsible for the low Ti, Nb and Ta concentrations (see Hofmann, 1988). The absence of high Zr and Ti concentrations, although both elements are mainly carried by the ultrastable heavy minerals zircon and rutile, can be explained by sorting during weathering or the minerals had been absent in the original rock source. However, only few is known about the geotectonic origin of rocks surrounding Stavanger and in Jæren, the region south of Stavanger (Fig. 1), in comparison to Karmøy (stippled area in Tig. 1); thus, interpretations of the non-mafic component in the samples are strongly hypothetical, but explain the differences in f.e. Cr/Th ratios compared to the mafic and ultramafic source rocks (Table 4).

Samples 11 and R7 are different from the others with less high Mg, Co, Ni and Cr concentrations but still comparable to normal shale or even above (Table 3; Fig. 5d, e, f). XRD data show that they contain significant less talc than the rest of the fragments, as well as large amounts of anthophyllite. R7 has higher $Al_2O_3$, $Ti_2O$, Ta, Nb, Zr, $K_2O$, $Na_2O$, LOI and TOC than all other samples, which points to the existence of rutile, zircon, feldspar and organic matter as observed by FE-SEM and reflected in TOC (Table 2). Alike R7 is sample 11 enriched in nearly all incompatible trace elements like Zr, Hf, light REE and Th, $Al_2O_3$ and $K_2O$ (Table 3; Fig. 5d). This points to a different composition of the pottery with a higher amount of felsic material than all other samples. Although samples R7 and 11 share a common characteristic with all other samples, namely the abundance of talc and asbestos-like mineral anthophyllite minerals, the two samples stand out in that the material composition is enriched in felsic components and might not be solely local. This is surprising, as the grave contexts with the two vessels are centrally
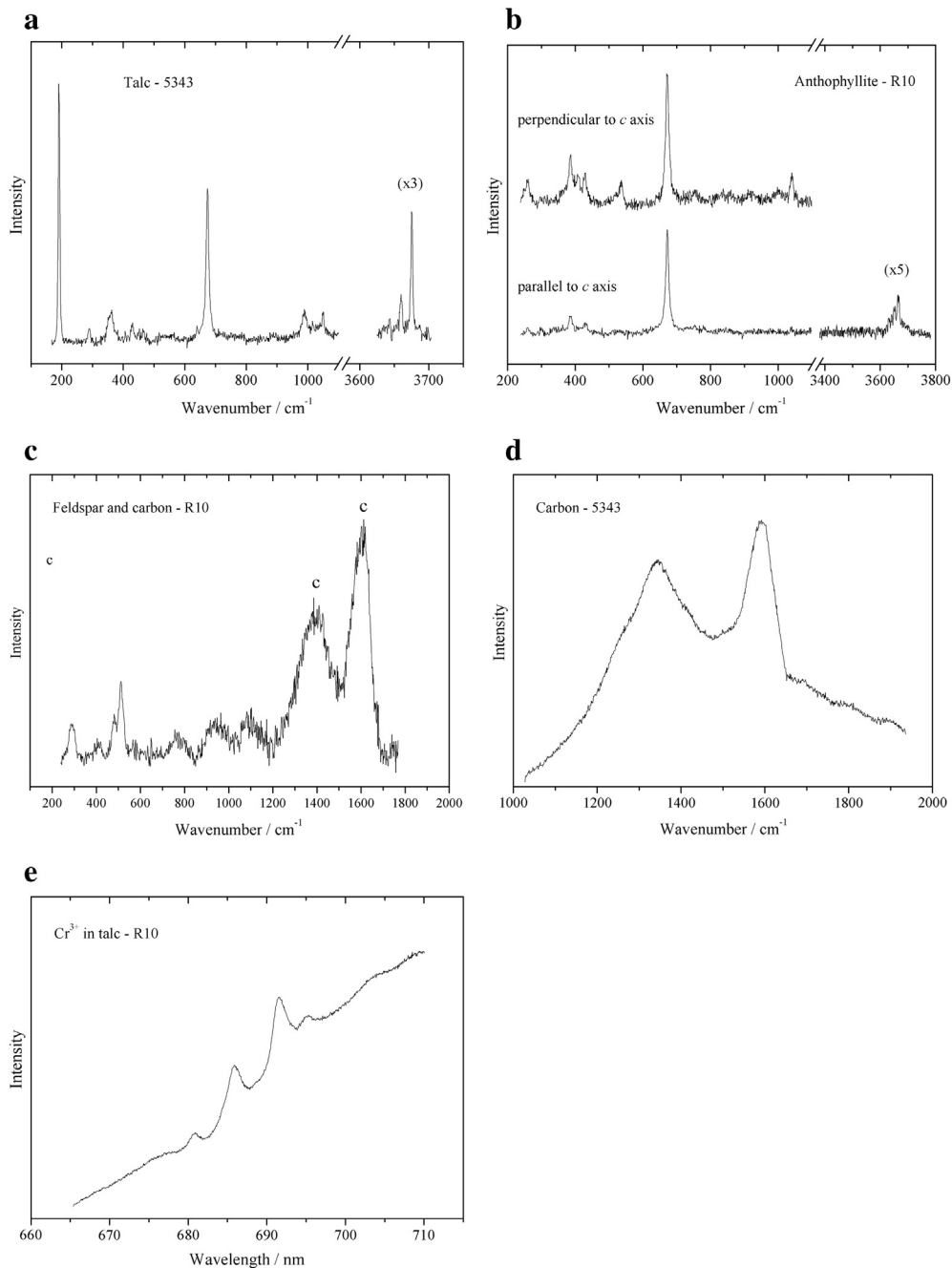
**Fig. 6.** Raman spectra of a) Low-frequency (100–1200 cm$^{-1}$), OH-stretching (3400–3800 cm$^{-1}$) regions of talc; b) Low-frequency (100–1200 cm$^{-1}$), OH-stretching (3400–3800 cm$^{-1}$) regions of anthophyllite; c) Feldspar with amorphous carbon; d) Amorphous carbon; e) Photoluminescence spectrum of Cr$^{3+}$ ions in talc.

located in a region rich with clays and additive minerals which are functional and of good quality. Also there is ample evidence for strong local potting traditions at the time of deposition, reflected in a rich distribution of locally produced pottery in settlements as well as in burial contexts (Fredriksen et al., 2014; Kristoffersen and Magnus, 2010).

The possibility that the area of Karmøy is the origin of the mafic to ultramafic component in the analyzed pottery may have impacts on the archeological interpretation of the grave and settlement contexts in which the material is found. This discussion, however, is not the focus of this contribution and awaits more detailed and further analytical work on a larger sample set. The use of materials for the pottery dominated by elongated relatively soft materials like talc and anthophyllite may also have some implication for the archeological context. Clearly, the extraordinary composition of the pottery with the high Cr and Ni (and Co) concentrations is characteristic for nearly all samples

and spectacular. The selection of this specific component is surprising as it does not bear any further advantage for the use of the pottery, besides possibly conductive advantages, which, however, has to be tested if correct. However, if the materials have been derived from Karmøy then this area might have had played an important role in the cultural context of the bucket-shaped pottery.

## 5. Conclusion

We report results from FE-SEM–EDS, geochemical data, mineralogical analyses and Raman spectroscopy of pottery of bucket-shaped ceramic from Rogaland (southwestern Norway) dated between the 5th and 6th Century. The study reveals a very rare pottery-type composed of asbestos–group minerals and an unusual enrichment in compatible elements like Cr (8–27× PAS), Ni (2–8× PAS) and Co (2–3× PAS)

**Table 4**
Comparison of the most important geochemical characteristics for the studied pottery. % = weight percent; ppm = parts per million; n.d. = not determined. Values for PAAS (Post-Archean Australian average shale) and UCC (typical Upper Continental Crust) and rocks of Karmøy as in Table 3.

| Sample | | | Zr/Ti | Nb/Y | Th/Sc | Zr/Sc | Cr/V | Cr/Th | Sc/Th | Y/Ni | MgO % | TiO$_2$ % | Cr ppm | Ni ppm |
|---|---|---|---|---|---|---|---|---|---|---|---|---|---|---|
| R2 | Grave | | 0.046 | 0.62 | 0.66 | 11.00 | 32 | 335 | 0.09 | 0.08 | 17.67 | 0.28 | 1539 | 120 |
| R6 | Grave | | 0.030 | 0.56 | 0.49 | 4.46 | 19 | 332 | 0.22 | 0.02 | 20.78 | 0.25 | 1628 | 439.4 |
| R7 | Grave | | 0.048 | 0.67 | 0.77 | 12.53 | 3 | 32 | 0.08 | 0.31 | 10.85 | 0.44 | 246 | 48 |
| R9 | Grave | | 0.030 | 0.51 | 0.63 | 5.83 | 20 | 172 | 0.17 | 0.03 | 16.52 | 0.29 | 978 | 397.4 |
| R10 | Grave | | 0.033 | 0.62 | 0.53 | 5.32 | 39 | 512 | 0.19 | 0.10 | 20.84 | 0.24 | 2456 | 109 |
| R12 | Grave | | 0.033 | 0.62 | 0.71 | 8.93 | 16 | 179 | 0.11 | 0.09 | 22.07 | 0.41 | 1143 | 133.8 |
| R14 | Grave | | 0.046 | 0.86 | 0.63 | 12.92 | 25 | 284 | 0.08 | 0.06 | 19.21 | 0.28 | 1081 | 121.5 |
| R15 | Grave | | 0.045 | 0.69 | 0.64 | 12.03 | 28 | 277 | 0.08 | 0.06 | 18.32 | 0.31 | 1245 | 129.8 |
| R18 | Grave | | 0.036 | 0.70 | 0.49 | 6.24 | 24 | 228 | 0.16 | 0.05 | 20.94 | 0.32 | 1232 | 222.3 |
| R29 | Grave | | 0.023 | 0.76 | 0.78 | 4.44 | 46 | 393 | 0.23 | 0.08 | 20.19 | 0.29 | 2750 | 106.3 |
| R31 | house hold | | 0.045 | 0.53 | 1.43 | 10.83 | 46 | 298 | 0.09 | 0.08 | 23.05 | 0.16 | 1697 | 88.6 |
| 11 | Grave | | 0.039 | 0.65 | 0.89 | 9.52 | 2 | 15.4 | 0.11 | 0.23 | 14.85 | 0.37 | 123 | 51.6 |
| 12 | Grave | | 0.031 | 0.61 | 0.39 | 3.83 | 20 | 248 | 0.26 | 0.09 | 19.37 | 0.33 | 1539 | 128.5 |
| PAAS and UCC | | | 0.035 | 0.70 | 0.91 | 13.13 | 1 | 7.5 | 0.08 | 0.49 | 2.20 | 1.00 | 110 | 55 |
| Karmøy | Gabbro | | 0.015 | 0.04 | 0.00 | 0.72 | 9 | 13467 | 1.38 | 0.03 | 8.53 | 0.31 | 808 | 210 |
| Karmøy | Gabbro | | 0.009 | 0.01 | 0.00 | 0.66 | 5 | 12220 | 1.52 | 0.07 | 9.68 | 0.47 | 611 | 148 |
| Karmøy | Dyke swarm | | 0.014 | n.d. | 0.00 | 0.38 | 7 | 6755 | 2.63 | 0.02 | 17.32 | 0.19 | 1351 | 271 |
| Karmøy | Dyke swarm | | 0.007 | n.d. | 0.01 | 0.38 | 7 | 5108 | 2.63 | 0.07 | 13.7 | 0.34 | 1277 | 177 |

carried by talc. XRD and Raman spectroscopy could reveal that Ni is introduced by a specific Ni-rich talc mineral and Cr occurs in a rare Cr-rich talc, both genetically related to ultramafic rocks. So far, we can only speculate if the talc phase is the same and contains sometimes Ni and in other case Cr or if these two phases are different mineral species. The pottery is also characterized further by high Mg concentrations between 10–20× PAS concentration, which reflects the high content of asbestos minerals and talc. The addition of Mg, Cr, Ni and Co and other compatible trace elements is, to our current knowledge, not caused by anthropogenic activity but related to the used materials, which are weathering products of mafic to ultramafic rocks. Rocks of this composition are exposed in vicinity of the sampling areas in a region called Karmøy, hosting a world famous ophiolite complex. The rock successions are perforated by mafic dykes and the intrusive contacts could easily be weathered to produce suitable mines/sources for pottery manufacturing.

The here reported composition is spectacular and extremely rare in pottery. Our study points out that as well unusual (even unsuitable?) material sources may have been used for pottery, and it can be speculated if these selections have been made by the manufacturers deliberately expressing a specific social function, or not, as sufficient 'ordinary', possibly to a greater extent more functional, clay materials are abundant in Rogaland.

## References

Andò, S., Garzanti, E., 2013. Raman spectroscopy in heavy-mineral studies. In: Scott, R.A., Smyth, H.R., Morton, A.C., Richardson, N. (Eds.), Sediment Provenance Studies in Hydrocarbon Exploration and Production. Geological Society, London, Special Publications 386 (http://dx.doi.org/10.1144/SP386.2).

Bersani, D., Andò, S., Vignola, P., Moltifiori, G., Marino, I.G., Lottici, P.P., 2009. Micro-Raman spectroscopy as a routine tool for garnet analysis. Spectrochimica Acta A 73, 484–491.

Bertolino, S., Galvan, Josa V., Carreras, A., Laguens, A., de la Fuente, G., Riveros, J.A., 2009. X-ray techniques applied to surface paintings of ceramic pottery pieces from Aguada culture (Catamarca, Argentina). X-Ray Spectrometry 38, 95–102.

Brindley, G.W., Maksimovic, Z., 1974. The nature and nomenclature of hydrous nickel-containing silicates. Clay Minerals 10, 271–277.

Bucher, K., Grapes, R., 2011. Petrogenesis of Metamorphic Rocks. Springer Heidelberg, New York, pp. 1–428.

Callender, E., 2003. 9.03 heavy metals in the environment—historical trends. In: Holland, H.D., Turekian, K.K. (Eds.), Treatise on geochemistry 9, pp. 67–105 (Lollar, B.S., Ed.).

De Waal, S.A., 1970. Nickel minerals from Barberton, South Africa: ii. Nimite, a nickel-rich chlorite. American Mineralogist 55, 18–30.

Degen, T., Sadki, M., Bron, E., König, U., Nénert, G., 2014. The high score suite. Powder Diffraction 29 (Suppl. S2), S13–S18.

Dilek, Y., Furnes, H., 2011. Ophiolite genesis and global tectonics: geochemical and tectonic fingerprinting of ancient oceanic lithosphere. Geological Society of America Bulletin 123, 387–411.

Floyd, P.A., Leveridge, B.E., 1987. Tectonic environment of the Devonian Gramscatho basin, south Cornwell: framework mode and geochemical evidence from turbidite sandstones. Journal of the Geological Society 144, 531–542.

Floyd, P.A., Winchester, J.A., Park, R.G., 1989. Geochemistry and tectonic setting of Lewisian clastic metasediments from the Early Proterozoic Loch Maree group of Gairloch, NW Scotland. Precambrian Research 45, 203–214.

Floyd, P.A., Keele, B.E., Leveridge, B.E., Franke, W., Shail, R., Dörr, W., 1990. Provenance and depositional environment of Rhenohercynian synorogenic greywackes from the Giessen Nappe, Germany. Geologische Rundschau 79 (3), 611–626.

Floyd, P.A., Shail, R., Leveridge, B.E., Franke, W., 1991. Geochemistry and provenance of Rhenohercynian synorogenic sandstones: implications for tectonic environment discrimination. In: Morton, A.C., Todd, S.P., Haughton, P.D.W. (Eds.), Developments in Sedimentary Provenance Studies. Geological Society Special Publication 57, pp. 173–188.

Fralick, P., 2003. Geochemistry of clastic sedimentary rocks: ratio techniques. In: Lentz, D.R. (Ed.), Geochemistry of Sediments and Sedimentary Rocks: Evolutionary Considerations to Mineral-Deposit-Forming Environments. Geological Association of Canada, GEOText 4, pp. 85–104.

Fredriksen, P.D., Kristoffersen, E.S., Zimmermann, U., 2014. Innovation and Collapse: Bucket-Shaped Pottery and Metalwork in the Terminal Migration Period. Norwegian Archaeological Review 47 (2), 119–140.

Furnes, H., Thon, A., Nordås, J., Garmann, L.B., 1982. Geochemistry of Caledonian metabasalts from some Norwegian ophiolite fragments. Contributions to Mineralogy and Petrology 79, 295–307.

Gomez, B., Neff, H., Rautman, M.L., Vaughan, S.J., Glascock, M.D., 2002. The source provenance of Bronze Age and Roman pottery from Cyprus. Archaeometry 44, 23–36.

Hofmann, A., 1988. Chemical differentiation of the Earth: the relationship between mantle, continental crust and oceanic crust. Earth and Planetary Science Letters 90, 297–314.

Hora, Z.D., 1997. Ultramafic-hosted chrysotile asbestos. Geological Fieldwork 1997, British Columbia Ministry of Employment and Investment, Paper 1998-1, 24 K-1 to 24 K-4.

Kleppe, E.J., 1993. On the provenance of bucket-shaped pottery. Acta Archaeologica 64, 293–300.

Kleppe, E.J., Simonsen, S.E., 1983. Bucket-shaped pots — a West-Norwegian ceramic form. Experiments with production methods. AmS-Skrifter 10. Arkeologisk museum Stavanger.

Kristoffersen, S., Magnus, B., 2010. Spannformete kar. Utvikling og variasjon. AmS-Varia 50. Arkeologisk museum, Universitetet i Stavanger.

Magnus, B., 1980. On the mending of bucket-shaped pots of the Migration Period in Norway. Studien zur Sachsenforschung 2. Hildesheim, pp. 275–288.

McLennan, S.M., 2001. Relationships between the trace element composition of sedimentary rocks and upper continental crust. Geochemistry, Geophysics, Geosystems 2 (2000GC000109).

McLennan, S.M., Taylor, S.R., McCulloch, M.T., Maynard, J.B., 1990. Geochemical and Nd-Sr isotopic composition of deep-sea turbidites: crustal evolution and plate tectonic associations. Geochimica et Cosmochimica Acta 54, 2015–2050.

McLennan, S.M., Hemming, S., McDaniel, D.K., Hanson, G.N., 1993. Geochemical approaches to sedimentation, provenance and tectonics. In: Johnsson, M.J., Basu, A. (Eds.), Processes Controlling the Composition of Clastic Sediments. Geological Society of America, Special Publication 284, pp. 21–40.

McLennan, S.M., Taylor, S.R., Hemming, S.R., 2006. Composition, differentiation, and evolution of continental crust: constrains from sedimentary rocks and heat flow. In: Brown, M., Rushmer, T. (Eds.), Evolution and Differentiation of the Continental Crust, pp. 92–134.

Pedersen, R.B., Hertogen, J., 1990. Magmatic evolution of the Karmoy ophiolite complex, relationships between MORB-IAT boninitic-calc-alkaline and alkaline magmatism. Contributions to Mineralogy and Petrology 104, 277–293.

Piper, D.Z., 1993. Seawater as the source of minor elements in black shales, phosphorites and other sedimentary rocks. Chemical Geology 114, 95–114.

Rudnick, R.L, Gao, S., 2003. 3.01 composition of the continental crust. In: Holland, H.D., Turekian, K.K. (Eds.), Treatise on Geochemistry 3, pp. 1–64 (Rudnick, R.L., Ed.).

Taylor, S.R., McLennan, S.M., 1985. The Continental Crust: its Composition and Evolution. Blackwell Scientific, Oxford, pp. 1–312.

Tveit, R., Furnes, H., Pedersen, R.B., 1993. Geological and geochemical development of the submarine volcanic sequence on Storøya, Leka ophiolite complex, North Trøndelag. Norsk Geologisk Tidsskrift 73, 81–94.

Veblen, D.R., 1980. Anthophyllite asbestos: microstructure, intergrown sheet silicates, and mechanism of fiber formation. American Mineralogist 65, 1075–1086.

Villanova-de-Benavent, C., Tredoux, M., Aiglsperger, T., Proenza, J., 2014. Ni-Mg-phyllosilicates from Bon Accord, Barberton, South Africa: new data on willemseite and nimite. 21st General Meeting of the IMA (IMA2014), Gauteng, South Africa, September 1–5; Abstract Volume, 212.

Winchester, J.A., Floyd, P.A., 1977. Geochemical discrimination of different magma series and their differentiation products using immobile elements. Chemical Geology 20, 325–343.

Zhou, J., Wang, X., Qiu, J., Gao, J., 2004. Geochemistry of Meso- and Neoproterozoic mafic-ultramafic rocks from northern Guangxi, China: arc or plume magmatism? Geochemical Journal 38, 139–152.